

X-ray CT in the detection of palm weevils

Andy K. W. Ma · Ali A. Alghamdi ·
Kassem Tofailli · Nicholas M. Spyrou

Received: 18 May 2011 / Published online: 31 May 2011
© Akadémiai Kiadó, Budapest, Hungary 2011

Abstract Early detection of the red palm weevils (RPW) is a major challenge in agriculture among all kinds of palm trees due to the nature of the insect and the difficulty to trace them through their life stages associated with the tree life. Many methods have been applied for the weevil detection such as X-ray diffraction techniques, fluoroscopy and ultrasound. On the other hand, the idea of tomography has been used for other purposes such as the determination of the age of the tree and for applied environmental studies. Such technology can also reveal the weevil in principle. In this study, we explore the use of X-ray CT for weevil detection with the Monte Carlo method. A model of the stem of a palm tree is developed for simulations. MCNPX is chosen to carry out the simulations for the radiography tally in the code. The tally records the 2D data of the X-ray beams irradiating the tree model. An iterative reconstruction method for cone beam CT is applied to obtain the 3D slices of the tree model. We are exploring the minimum number of projection angles and the detectability of the weevil. We shall also report the sensitivity of weevil detection using X-ray CT with a large set of simulations with different weevil sizes and tree diameters.

Keywords Palm tree · Red palm weevil · Pest control · Early detection · CT · Monte Carlo

Introduction

The infestation of red palm weevil (*Rynchophorus ferrugineus*) in the palm trees is a serious agricultural problem in North Africa and the Middle East. The pest is particularly damaging in the date palms because the date palm is an important fruit crop in the region. It was estimated that the RPW infestation can cause as much as 20% loss in the crops [1]. It was first recorded in coconuts in Southeast Asia [2]. The weevil first appeared in the Persian Gulf countries in 1986. It then spread across the Gulf to Iran and across the Arabian Peninsula and the Red Sea to Egypt and North Africa by 1993 [3]. It is now found in most Middle East countries. The first incident of the RPW, a dead adult, reaching the United States was reported in 2010 [4]. Although the adult RPW is a strong flyer, the fast spreading of the pest is associated with the transportation of the young and adult trees. The infested trees are often destroyed, either by being consumed by the undetected weevils or burned down after the weevils have been discovered. Early detection of the presence of the RPW could mean a significant save in the capital and labour investment in the plantations.

The RPW is a type of beetles. A female RPW can lay about 200 eggs [5] at the bases of the leaves and at the open wounds in the tree stem. On average, each egg is 0.26 cm in length and 0.11 cm in diameter [6]. The larvae are hatched after about 3 days [7] and they bore themselves deep into the tree where the soft fibres are. The larval stage lasts about 43 days [7] during that period the larva grows to 5 cm long and 2 cm in diameter [6] when they come out of

A. K. W. Ma (✉) · A. A. Alghamdi
Department of Radiological Sciences, College of Applied
Medical Sciences, University of Dammam, Dammam, Saudi
Arabia
e-mail: andyma@physics.org

K. Tofailli
Agriculture Medical Solutions, Ltd., Hayes, Middlesex, UK

N. M. Spyrou
Centre of Nuclear and Radiation Physics, Faculty of Engineering
and Physical Sciences, University of Surrey, Guildford, UK

the tree for pupation. The adult beetle does not move onto another tree while there are soft fibres remaining in the tree. Therefore, different stages of the RPW can be found in the same tree. The presence of adults is an indication of infestation. Successful pheromone traps of several species of the adult palm weevils have been reported [5, 8, 9]. The method is widely used by governments in the protocol to control the movement of palm trees [10].

Other methods have been investigated to detect the RPW directly and early, ranging from acoustic method with signal processing algorithms [1], neutron activation of cerium-labelled larvae [11] and neutron radiography [12] to using trained dogs to find the RPW [13]. Ultrasound and X-ray-based techniques have also been explored [14]. However, each method has its own strength and weaknesses. An effective direct detection of the larvae inside the palm tree remains to be devised.

Computed tomography (CT) is a well-known technique applied in medical diagnosis with great success in the last four decades. CT images are reconstructed from 2D projections that are obtained continuously over a full circle around the patient. However, it is possible to obtain a pseudo-3D image from a finite number of projections as in the case of digital tomosynthesis [15]. Another development in medical imaging is the use of dual-energy imaging. Dual energy subtraction images have been demonstrated in enhancing low-contrast images in mammography [16]. In this study, we explored the use of X-ray CT with finite number of projections in the weevil detection. Furthermore, we also explored the idea of dual-energy CT as a means to enhance to the low-contrast images. The work was carried out as a Monte Carlo study. A model of the tree stem was developed for the purpose.

Experimental

MCNPX [17] was chosen to carry out the simulations. MCNPX is capable of tracking photons, electrons, neutrons, protons and other subatomic particles. Only the photon tracking is selected in this study. Electrons are ignored to decrease the simulation time. Other particles are not produced in the energy range of our study. In photon tracking, the code accounts for photoelectric absorption, Rayleigh scattering and Compton scattering. Pair production does not occur in the energy range for imaging. The radiography tally in MCNPX, estimates the average number of particles reaching the tally elements that are arranged in a two-dimensional grid. The grid is positioned orthogonal to the axis of the X-ray beam. The arrangement of the beam and the radiography tally models a digital imaging system in radiography.

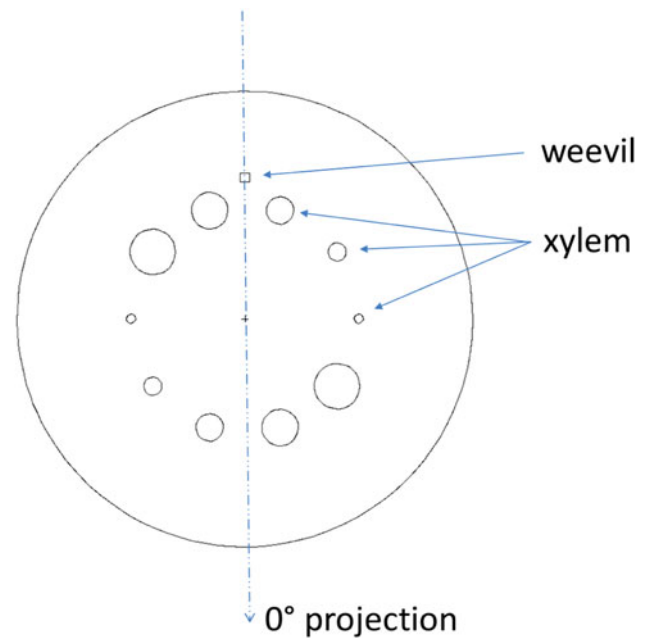


Fig. 1 Cross section of the palm tree model with weevil

The model of the tree stem was composed of a series of cylinders (Fig. 1). The outer cylinder of 10 cm diameter represents the tree stem. The smaller cylinders inside are the xylems with diameters from 0.2 cm to 1 cm. The weevil is 0.2 mm × 0.2 mm × 0.4 mm. This is the size of a weevil soon after hatching. The tree stem is assumed to be made up of cellulose that is long chain sugar molecules. The elemental composition of sugar is used in the simulation. The density of the tree stem is 0.9 g/cm³. The proximate composition of the weevil for late-stage larvae [18] is used to derive its elemental composition and density (Table 1). In the derivation of the elemental composition, it was assumed that the crude fibre and the protein are of similar composition to the muscle protein in NIST Physics Reference Data [19] and that the crude fat is similar to the NIST adipose tissues. The density ρ of the weevil was also derived from the proximate composition using Eq. 1

$$\rho = \frac{\rho_{\text{water}}\rho_{\text{fat}}\rho_{\text{protein}}}{m_{\text{water}}\rho_{\text{fat}}\rho_{\text{protein}} + m_{\text{fat}}\rho_{\text{water}}\rho_{\text{protein}} + m_{\text{protein}}\rho_{\text{water}}\rho_{\text{fat}}} \quad (1)$$

where ρ_{water} , ρ_{fat} and ρ_{protein} are the densities of water, fat and protein and m_{water} , m_{fat} and m_{protein} are the mass fractions of water, fat and protein in the proximate composition. We assumed the densities from NIST for fat and protein in the calculation. The density thus obtained was 0.95 g/cm³.

The density was estimated again from the weevil mass and dimension. Assuming that half of the weevil body is a truncated circular paraboloid, its density ρ was given by Eq. 2

Table 1 Proximate composition [18] and derived elemental composition of the red palm weevil

Material	Mass fraction
Proximate Composition	
Moisture	0.0840
Ash	0.0233
Crude fat	0.6213
Crude fibre	0.1722
Protein	0.1051
Carbohydrate	0.0782
Derived elemental composition	
Hydrogen	0.114
Carbon	0.397
Nitrogen	0.013
Oxygen	0.472
Chlorine	0.002
Sodium	<0.001
Magnesium	<0.001
Sulphur	<0.001
Potassium	<0.001
Calcium	<0.001
Iron	<0.001
Zinc	<0.001

The largest standard deviation is 10% in the proximate composition. This is also assumed in the elemental composition

$$\rho = \frac{m}{\pi l (r_{\text{body}}^2 - r_{\text{head}}^2)} \quad (2)$$

where m , and l are the mass and half length of the weevil; r_{body} and r_{head} are the half width of the weevil body and its head. The sample weevil in reference [18] weighed 8.14 ± 0.14 g and measured 4.61 ± 0.06 cm long; its body width was 2.05 ± 0.04 cm and its head 1.10 ± 0.01 cm. These data give a density of 0.90 g/cm³ to the weevil. However, this second value is probably an under-estimation because we assumed that the weevil had a circular cross section and its calculated volume was over-estimated. Thus the value 0.95 ± 0.05 g/cm³ was chosen as the estimation of the weevil density.

Since this is a preliminary study, simulations were carried out at with mono-energetic beams. Two energies were simulated –25 and 50 keV. The energy of each beam is interpreted as an approximate to the average beam energy. The angle between projections varied from 2° to 5°. The imager modelled by the radiography tally was 10 cm × 10 cm with 200 elements in each dimension, that is, each detector element is 0.5 mm × 0.5 mm. The 0° projection in this study corresponds to the vertical projection in Fig. 1 such that the X-ray source is closest to the weevil while the imager is on the opposite side of the palm tree stem. A total

of 504 simulations were performed. Each simulation gives a 2D projection image of the palm tree model in a matter of minutes with a desktop computer. The collection of 2D projections was reconstructed into a 3D image. The reconstruction was carried out with OSCaR [20], a cone-beam CT reconstruction tool that uses the filtered back-projection method. The reconstructed voxel dimensions were of 0.3 mm × 0.3 mm × 0.3 mm.

Results and discussion

On a computer screen, the weevil in a projection image (at 50 keV and 0° projection angle) is visible after carefully adjusting the contrast and brightness. It must be noted that the lack of superimposing xylems in the projection image at 0° helps in the visibility of the weevil. At other projection angles, the weevil is not normally detectable. A slice of the corresponding reconstructed 3D image is in Fig. 2. In the projection images at 25 keV, the situation is similar except that the grey scale window is even more difficult to set for the weevil detection.. This visibility will further be degraded in a real system due to the differing noise characteristics between a simulated image and one in a real system as explained in the next section. Figure 3 is a subtracted image from reconstructed images at 25 and 50 keV. The weevil is clearly visible in this image. When the angle between projections was increased to 5° to reduce the number of projections, the reconstructed image did not have the power to resolve the weevil. More importantly,

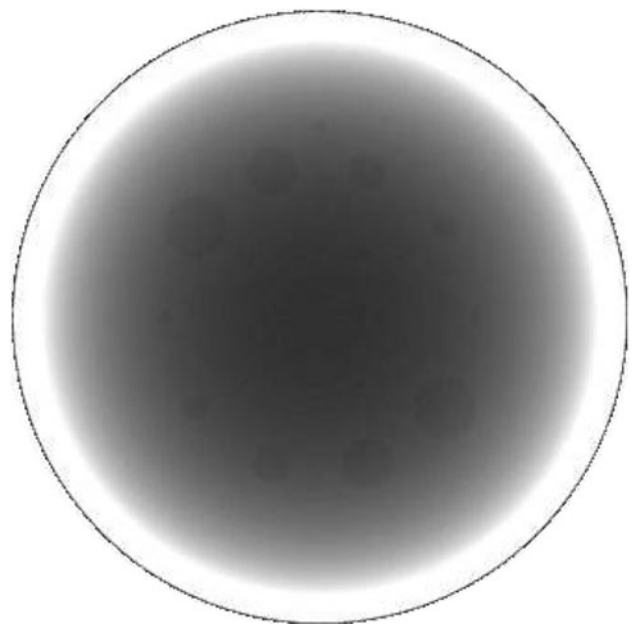


Fig. 2 A reconstructed cross section of the palm tree model at 50 keV. The weevil becomes much clearer than in a projection image

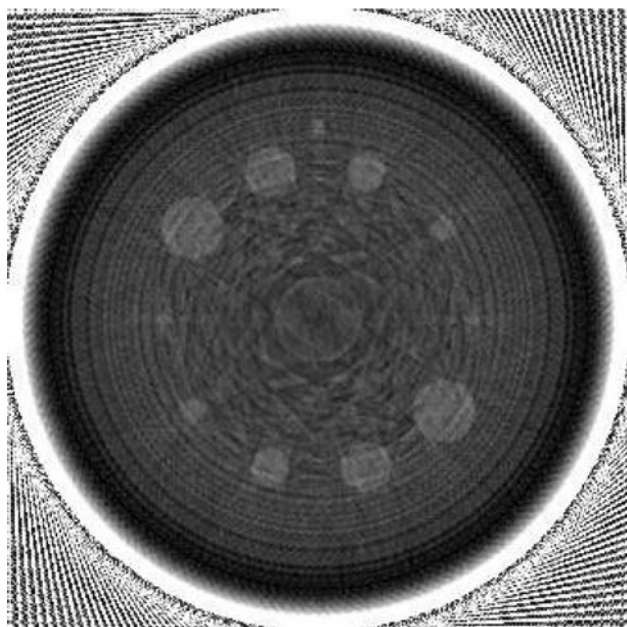


Fig. 3 The subtracted image from the cone beam reconstruction obtained at 50 keV and that at 25 keV. The weevil is the clearest

the dual energy enhancement did not offer any advantage either. Therefore, the maximum angle between projections is certainly less than 5° .

Since the radiography tally estimates the average number of photons arriving at an imager element, there is very little noise compared to a real system. Furthermore, the statistical fluctuation in the image is associated with the precision of the Monte Carlo simulation which is related to the number of histories. This fluctuation is not associated with the tube current or mAs of the X-ray tube. In fact, it is independent of the mAs. The simulated image may be interpreted as one obtained at high mAs—“high” in the sense that the resultant image is essentially noise free. Noise is a major factor in reading and interpreting radiographic images. This is especially true in low-contrast images. It affects the detectability of small foreign objects hidden in a body. In the case of medical imaging, radiographers must strike a balance between obtaining a low-noise image and the radiation dose to the patient. However, this balance is more in favour of obtaining low-noise images in the case palm weevil detection. When applied in the field, relatively high mAs may be employed; low-noise images are producible. If we take into account the probable degradation of image quality due to noise in real situation, the maximum angle between projections is likely to be 2° using filtered back-projection reconstruction method.

At the energy range in this study, photoelectrons and Compton recoil electrons of low energy will be generated. Although they have finite range and tend to blur the image, electron tracking was turned off for the sake of computing

efficiency. At 50 keV, the continuous slow-down approximation (CSDA) range of an electron in water is less than 0.05 mm. This is one order of magnitude smaller than the pixel dimension of digital imagers, typically around 0.5 mm. Only at energies above 120 keV does the CSDA range of the electron become comparable to the pixel size. Depending on the density of the imager material, the CSDA range may decrease significantly due to the high stopping power of the imager material as compared to water. Therefore the blurring caused by the electrons can be ignored. A second issue concerning electron tracking is in the quantum noise of the image. This is especially important at low tube current (low mAs). However, the possibility high mAs as explained in the previous paragraph also justifies our simulations without electron tracking and in conjunction with the radiography tally.

We did not carry out the simulation of a continuous CT beam for several reasons. First of all, the continuous beam is more difficult to simulate given that MCNPX was used. The code does not have a model for a continuously moving detector. Although we could have approximated the continuous movement by increasing the number of projections with small steps in the projection angle, this time-consuming exercise was deemed unnecessary—if a finite number of projections allow the detection of small weevils, the continuous beam will only improve the detection limit. Thus it is unnecessary to demonstrate the continuous beam would be better. More importantly, a continuous beam requires a dedicated CT machine to handle palm trees that are substantially larger than patients in hospital. Discrete beams allow the conversion of existing X-ray equipment into a cone-beam CT machine by either mounting the X-ray tube and the imager on a C-arm or by rotating the palm tree between the tube and imager. Hence the technique has the potential to be deployed easily and quickly in the field.

The grey scale in the reconstructed image is associated with the CT number and tissue density. Thus, the assumptions in the elemental compositions and densities are the sources of uncertainty in the simulations. The density of protein reported in literature varies between 1.2 and 1.5 g/cm^3 and it depends on the molecular weight of the protein. It also depends on the purity of the protein sample. It is unlikely that the proximate composition in reference [18] does not even contain a layer of water molecule in their protein sample. A high value of density is unsuitable in our derivation of the density of the weevil. Because of the uncertainty concerning the protein, we decided to group the protein and crude fibre together and to approximate the mixture with the NIST data for muscle. In fact, using 1.44 g/cm^3 for pure protein in Eq. 1 will give 1.09 g/cm^3 as the density of the weevil. This justifies our estimated density of $0.95 \pm 0.05 \text{ g}/\text{cm}^3$. Should the protein

density be higher than our assumed value, the contrast in the con-beam CT images would be only improved over our synthetic images.

The weevil and palm tree model in our simulations represents a small weevil (2 mm wide). This is the size of a weevil soon after hatched from the egg. Together with the discussion of the density of protein above, our work was an attempt to produce the lower limit of weevil detectability, that is, simulations with the smallest and lightest possible weevil and the maximum angle between projections. Although the projection images and the cone-beam CT may not be the best solution, dual-energy subtraction *can* enhance the low contrast weevil and provide a solution to directly detect the weevil in the palm tree.

Conclusions

As mentioned in previous section, there were many assumptions in the simulations. Further work must be carried out to address the issues in the assumptions. More realistic simulations and experiments will be performed to validate the results of this work. Future simulations will include polyenergetic beams with the X-ray anode and filter taken into account. Modelling of the imager can be improved to incorporate noise characteristics from different mAs. Such simulations may be used to optimise the cone-beam CT system configuration.

We have presented the simulations of cone-beam CT applied in RPW detection. Furthermore, we demonstrated that the cone-beam CT reconstruction from a finite number of projections may be sufficient for the detection of the weevil. We have determined that the angle between projections is likely to be at 2° for filtered back-projection reconstruction method. More importantly, the technique is applicable in the field with minimal modification of existing X-ray equipment. The weevil size in the simulations was small—about the size of a weevil soon after hatching. The size was so chosen that if it can be detected, larger ones can be too. In other words, we were simulating the *early* detection of the weevils using cone-beam CT technique.

References

- Hussein WB, Hussein MA, Becker T (2010) Detection of the red palm weevil *Rhynchophorus ferrugineus* using its bioacoustics features. *Bioacoustics* 19:177–194
- Faleiro J (2006) A review of the issues and management of the red palm weevil *Rhynchophorus ferrugineus* (Coleoptera: Rhynchophoridae) in coconut and date palm during the last one hundred years. *Int J Trop Insect Sci* 26:135–154
- Kehat M (1999) Threat to date palms in Israel, Jordan and the Palestinian authority by the red palm weevil, *Rhynchophorus ferrugineus*. *Phytoparasitica* 27:241–242
- NAPPO Phytosanitary Alert System (2010) <http://www.pestalert.org/oprDetail.cfm?oprID=468>. Accessed 2 Mar 2011
- Ferry M, Gómez S (2003) The red palm weevil in the Mediterranean area. *Palms* 46:4
- Red Palm Weevil (2008) <http://www.redpalmweevil.com/newlook/index2.htm>. Accessed 2 Mar 2011
- Hagley EAC (1965) On the life history and habits of the palm weevil, *Rhynchophorus palmarium*. *Ann Entomol Soc Am* 58:22–28
- Alpizar D, Fallas M, Oehlschlager AC, Gonzalez LM, Chinchilla CM, Bulgarelli J (2002) Pheromone mass trapping of the West Indian sugarcane weevil and the American palm weevil (Coleoptera: Curculionidae) in *Palmito palm*. *Fla Entomol* 85:426–430
- Perez AL, Gries G, Gries R, Giblin-Davis RM, Oehlschlager AC (1994) Pheromone chirality of African palm weevil, *Rhynchophorus phoenicis* (F.) and palmetto weevil, *Rhynchophorus cruentatus* (F.) (Coleoptera: Curculionidae). *J Chem Ecol* 20: 2653–2671
- Bertone C, Michalak PS, Roda A (2010) New pest response guidelines—red palm weevil *Rhynchophorus ferrugineus*. United States Department of Agriculture, Riverdale
- Rahalkar GW, Mistry KB, Harwalkar MR, Bharathan KG, Gopal-Ayengar AR (1971) Labeling adults of red palm weevil (*Rhynchophorus ferrugineus*) with cerium for detection by neutron activation. *Ecology* 52:186–188
- Alghamdi AA (2011) Neutron tomography for palm weevil detection. In: The 13th conference on modern trend in activation analysis, 13–18 March 2011, College Station, Texas, USA
- Nakash J, Osem Y, Kehat M (2000) A suggestion to use dogs for detecting red palm weevil (*Rhynchophorus ferrugineus*) infestation in date palms in Israel. *Phytoparasitica* 28:153–155
- Tofailli K (2010) The early detection of red palm weevil: a new method. In: Fourth international date palm conference, 15–17 March 2010, Abu Dhabi, United Arab Emirates
- Dobbins JT, Godfrey DJ (2003) Digital X-ray tomosynthesis: current state of the art and clinical potential. *Phys Med Biol* 48:R65–R106
- Johns PC (1985) Theoretical optimization of dual-energy X-ray imaging with application to mammography. *Med Phys* 12: 289–296
- Pelowitz DB (2005) MCNPXTM user's manual. Los Alamos National Laboratory, Los Alamos
- Omotoso O, Adedire C (2007) Nutrient composition, mineral content and the solubility of the proteins of palm weevil, *Rhynchophorus phoenicis* f. (Coleoptera: Curculionidae). *J Zhejiang Univ Sci B* 8:318–322
- NIST Physical Reference Data. <http://www.nist.gov/pml/data/index.cfm>. Accessed 7 Mar 2011
- Rezvani N, Aruliah D, Jackson K, Moseley D, Siewerdsen J (2008) OSCaR, an open source cone-beam CT reconstruction tool for imaging research